Turbulent thermal convection at high Rayleigh numbers for a Boussinesq fluid of constant Prandtl number

G. Amati, K. Koal, and F. Massaioli
CASPUR Via dei Tizii 6/b, 00185 Roma, Italy

K. R. Sreenivasan
International Centre for Theoretical Physics, Strada Costiera 11, 34014 Trieste, Italy

R. Verzicco[a]
Politecnico di Bari, DIMeG and CEMeC, Via Re David 200, 70125 Bari, Italy

The results from direct numerical simulations of turbulent Boussinesq convection are briefly presented. The flow is computed for a cylindrical cell of aspect ratio 1/2 in order to compare with the results from recent experiments. The results span eight decades of Ra from 2×10^6 to 2×10^{14} and form the baseline data for a strictly Boussinesq fluid of constant Prandtl number (Pr $=0.7$). A conclusion is that the Nusselt number varies nearly as the $1/3$ power of Ra for about four decades towards the upper end of the Ra range covered. © *2005 American Institute of Physics*. [DOI: 10.1063/1.2140023]

Motivated by applications in astrophysics, geophysics, as well as industry, experimental research in thermally driven convective turbulence has been aiming for the largest possible Rayleigh numbers (Ra) in the well-controlled Rayleigh-Bénard problem.[1–7] In the applications just cited, Ra is estimated[8] to vary from 10^6 to 10^{22}, and so there is much interest in covering a similarly wide range of Ra in experiments. However, such experiments have had to contend with several artifacts such as the effects of sidewall conduction[9–12] at low Ra, the difficulties of maintaining the constant-temperature conditions at the bottom and top plates,[13,14] non-Boussinesq effects,[3,5,6] variable Prandtl numbers,[3–7] and so forth. Plausible corrections for these effects have been invented in the references just cited, but their approximate nature makes it difficult to rely on them fully, especially when the artifacts occur in combination. These limitations have made it difficult to be precise about the scaling law of heat transport at high Rayleigh numbers.

Impressive advances of the CPU architectures and parallel computing in the last decade have made the direct numerical simulation (DNS) of the Rayleigh-Bénard problem an attractive option, especially on two counts. Simulations can (a) avoid several technological limitations just discussed and provide baseline data, and (b) obtain flow details that are inaccessible, despite impressive gains,[15] in experiments. Here, we perform the DNS of governing field equations covering $2 \times 10^6 \leq \mathrm{Ra} \leq 2 \times 10^{14}$. The calculations pertain to Pr $=0.7$, strict Boussinesq conditions, constant temperature for bottom and top plates, and no sidewall conduction. We consider the flow in a cylindrical cell of aspect ratio $\Gamma=1/2$, with no-slip surfaces, heated from below and cooled from above, and with an adiabatic sidewall. This paper is a first report of the principal results on heat transport. In the Pr-Ra phase plane, we cover the region IV_u of Ref. 16, but

the boundary layers undergo a change in character from being nominally laminar to becoming turbulent.

The flow is solved by numerically integrating three-dimensional Navier-Stokes equations with Boussinesq approximation. The numerical method is already described in Ref. 17, and it suffices here to mention that the equations in cylindrical coordinates are solved by central second-order accurate finite-difference approximations in space and time.

The present simulations consist of nine runs at Pr$=0.7$ and $2 \times 10^6 \leq \mathrm{Ra} \leq 2 \times 10^{14}$. Those in the range $2 \times 10^6 - 2 \times 10^{11}$ are from Ref. 17 and the flow at Ra$=2 \times 10^{11}$ has been recomputed with a finer spatial resolution as a check for the higher-Ra flows. The cases $2 \times 10^{12} \leq \mathrm{Ra} \leq 2 \times 10^{14}$ are new. All simulations were run on multiprocessor IBM Power3, Power4, and NEC SF-6+ machines of the computing center CASPUR in Rome, and the entire project needed about 2×10^5 IBM Power4-equivalent CPU hours.

The smallest velocity and temperature lengths in the bulk are nominally the Kolmogorov scale η and the Corrsin scale η_θ. The smallest scales near the plates are controlled by the boundary layer thicknesses δ_u (velocity) and δ_θ (thermal). Since Pr$=0.7$, $\eta_\theta \approx \eta$ and $\delta_\theta \approx \delta_u$. Thus, the grid size must be of the order of η in the bulk and resolve the boundary layers on the plates. All the relevant scales can be estimated *a priori* by existing empirical scaling relations for the Nusselt number (Nu) versus Ra as confirmed *a posteriori* by Verzicco and Camussi.[17] Grötzbach[18] estimates that $\eta \sim h(\mathrm{Pr}^2/\mathrm{Ra}\,\mathrm{Nu})^{(1/4)}$, where Nu is the total heat flux normalized by the purely conductive value, and h is the vertical distance between the horizontal plates and suggests that it is enough to resolve with four grid points the thermal boundary layer $\delta_\theta \approx h/(2\mathrm{Nu})$. He proposes that this can be checked by monitoring Nu.

To explore the optimal grid, we performed simulations of selected cases for several resolutions. Simulations of Verzicco and Camussi[17] for Ra$=2 \times 10^7$, using grid resolution in the bulk of $\eta/2.4$, and 10 points in the thermal boundary

---

[a]Author to whom correspondence should be addressed. Telephone: 39 0805963898. Fax: 39 080 5963411. Electronic mail: verzicco@poliba.it
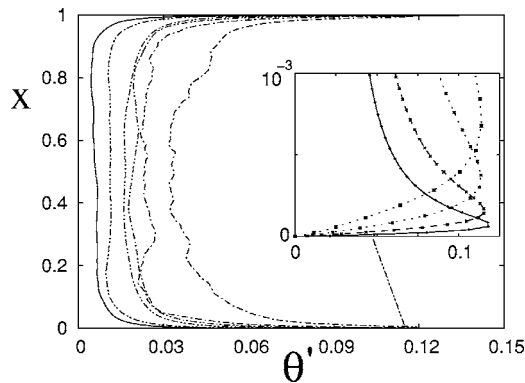
17, 121701-1

FIG. 1. Root-mean-square temperature profiles in the vertical direction x, averaged over time, and the azimuthal orientation, for different Rayleigh numbers; the inset is a zoom of the lower wall region to emphasize the wall resolution (with the symbols representing the positions of the grid points). From left to right, the lines are for (—) $Ra=2\times10^{14}$ and (–·–) $Ra=2\times10^9$ decreasing by factors of 10. Temperatures are normalized by the total temperature difference $\triangle$.

FIG. 2. (a) Compensated Nusselt number vs the Rayleigh number. (b) Ra-Pr phase diagram for the mean flow structure: region $1R$ stands for a single recirculation, $2R$ for two rolls; no mean flow occurs in the region NMF. (●) Present results; (×) data from Niemela *et al.* (Ref. 5); (○) data from Chavanne *et al.* (Ref. 6).

layer, had yielded $Nu=20.24\pm1.42$, while resolutions of five points within the thermal boundary layer, and of 4η in the bulk, had yielded $Nu=20.56\pm1.48$. Accordingly, the case of $Ra=2\times10^{11}$ was earlier computed by Verzicco and Camussi[17] with the grid in the bulk that is 4η in size, containing five points in the thermal boundary layer. We have recomputed the same flow with the mesh in the bulk of 1.2η and with 10 points in the thermal boundary layer, obtaining $Nu=440.3\pm10$; this is to be compared with the previous result $Nu=447.2\pm11.7$. Such considerations allowed us to scale up the simulations for the three highest Rayleigh numbers for which the following details pertain. For $Ra=2\times10^{12}$ the number of nodes was $257\times193\times769$ in the azimuthal, radial, and vertical directions with a maximum grid spacing in the bulk of $\Delta_{max}\simeq2.4\eta$ and a near-wall resolution $\Delta_{min}\simeq\delta_\theta/8$. For $Ra=2\times10^{13}$, the same numbers were $385\times301\times1381$, $\Delta_{max}\simeq2.3\eta$, $\Delta_{min}\simeq\delta_\theta/120$, while for $Ra=2\times10^{14}$ we used $513\times401\times1801$, $\Delta_{max}\simeq2.2\eta$, $\Delta_{min}\simeq\delta_\theta/38$.

For the data of Fig. 1, the near-wall resolution ranges from seven nodes in the thermal boundary layer at $Ra=2\times10^{14}$ to 12 nodes at $Ra=2\times10^{13}$. Such a fine spatial resolution requires an equally fine time step in order to capture the dynamics of the smallest scales. We have found that the needed time step depended on Ra and, in particular, up to 7000 time steps for the turnover time of each large eddy have been used at $Ra=2\times10^{14}$ and 2000 steps at $Ra=2\times10^{12}$. The simulations at $Ra=2\times10^{12}$ were run for 110 turnover times while those at $Ra=2\times10^{13}$ and $Ra=2\times10^{14}$ were limited to 40 turnover times. It was found that the statistics at the end of the simulation were close to those computed at 3/4 and 4/5 of the total simulation times, respectively.

The Nusselt number is plotted in Fig. 2(a) as a function of Ra; in order to make the scaling more evident, Nu has been compensated by the factor $Ra^{1/3}$. The relation $Nu\sim Ra^{1/3}$ over more than four decades in Ra brings back the theoretical analysis[19] to about 50 years ago, when Malkus and Priestley predicted it by assuming that all the heat transfer occurred within the thermal boundary layers, the bulk of
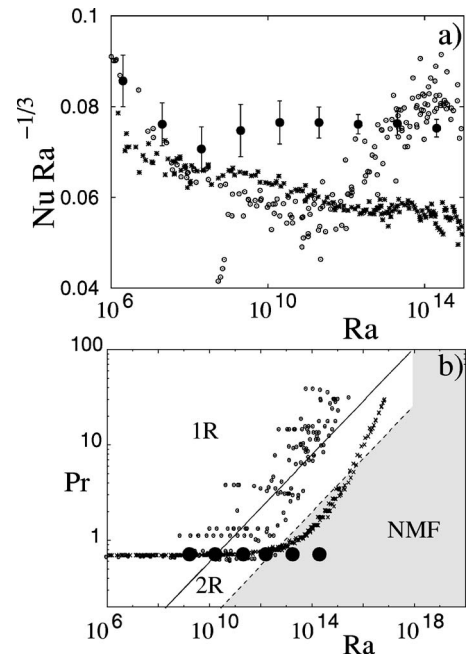
the flow was essentially isothermal, and that the thermal boundary layers did not communicate through the bulk. The first two hypotheses have been confirmed by laboratory experiments as well as by numerical simulations, and thus accepted. The independence of the two thermal boundary layers, in contrast, has been refuted often owing to the presence of a persistent large-scale recirculation which connects the top and bottom plates, presumably reinjecting the height between the plates as an additional length. We will show below that, for the present cylindrical cell of aspect ratio $\Gamma=1/2$, the large-scale flow does not survive (or, at least, substantially weakens) beyond $Ra\approx10^{12}$, thus making it possible for the thermal boundary layers to be essentially independent of each other. The 1/3 power seems to be appropriate for at least these conditions.

The occurrence of the 1/3 power was already noted in previous numerical simulations[17] and in recent experiments[12,20] though, in Ref. 20, it applied for slightly less than a decade of Ra in small aspect ratio cylindrical cells ($\Gamma=0.43$, 0.67, and 0.98). Unpublished data of Niemela and Sreenivasan (private communication) for aspect ratio 4 have shown a closely similar result. The Nusselt numbers from simulations, shown in Fig. 2(a), differ slightly from experimental values. These differences are unlikely to be due to insufficient spatial resolution in simulations because it would lead to underestimated temperature gradients at the wall and to smaller Nu. The differences between experiments may in part be due to different degrees of departure from perfect constancy of the wall temperatures. In part, the differences might also be caused by differences in the mean flow structure.[12] According to the model of Stringano and Verzicco,[21] these structural changes can be described by the
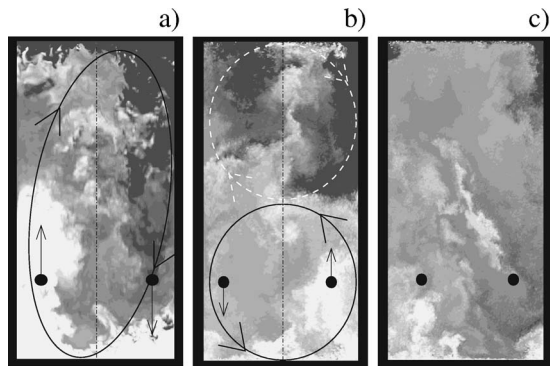
FIG. 3. Snapshots of temperature showing the possible mean flow configurations: (a) single recirculation Ra=2×10^{10} [region $1R$ of Fig. 2(b)]; (b) the two-roll configuration Ra=2×10^{12} [region $2R$ of Fig. 2(b)]; (c) only turbulent fluctuations Ra=2×10^{14} [region NMF of Fig. 2(b)]. Only the temperature range $0.475 \leq \theta \leq 0.525$ is represented with shades of gray; light gray stands for warm fluid and dark gray for cold fluid.

FIG. 4. Time series of vertical velocity sampled in the positions sketched in Fig. 3: (a) Ra=2×10^{10}, (b) Ra=2×10^{12}, (c) Ra=2×10^{14}. Velocities are normalized by the free-fall velocity $U = \sqrt{g \alpha \Delta h}$.

phase diagram of Fig. 2(b) in the Ra-Pr plane. The consistency of this model has been verified by sequences of visualizations such as those of Fig. 3 and three-dimensional animations. Even from single snapshots, it is possible to distinguish the structure of the large-scale flow via the presence (or absence) of warm and cold currents.

To quantify the differences in the flow structure, we show sample vertical velocities in Fig. 4 and compute their statistics in Fig. 5. For the cases represented by Figs. 3(a) and 3(b), the velocity signals should be anticorrelated and possess a negative average. For the configuration of Fig. 3(c), no mean flow is present and the two velocity signals should not be correlated. These conclusions, supported qualitatively from velocity time series in Fig. 4, are confirmed quantitatively in Fig. 5. This figure shows the probability density function of the product between the two velocities and the time-averaged maximum vertical velocity. The histograms of the velocity product in Fig. 5(a) show large negative tails at Ra=2×10^{9} and Ra=2×10^{10}, weaker negative tails at Ra=2×10^{11} and 2×10^{12}, and symmetric tails at Ra=2×10^{13} and Ra=2×10^{14}, in agreement with the depiction of Fig. 2(b). The inset of Fig. 5(a) clearly shows that in the high end of Ra the mean value of the histograms tends to zero thus indicating uncorrelated velocities over the extent of the computational domain. The transition to different flow structures is also consistent with Fig. 5(b), which shows the maximum vertical velocity as a function of Ra. In fact, considering that for a given temperature difference the maximum vertical velocity is proportional to the distance along which a fluid particle can accelerate, it is apparent that the configuration of Fig. 3(a) produces the largest velocities while that of Fig. 3(c) yields the smallest, and the velocity keeps decreasing with Ra owing to the dominance of smaller flow scales.

The changes in the mean flow structure have an impact also on the viscous boundary layers on the horizontal plates. A short discussion of the boundary layer structure is useful because it has been assumed[16,22] that they quantitatively behave as "standard" laminar (Blasius) and turbulent boundary layers on a flat plate. As shown in Fig. 6(a), the intensity of
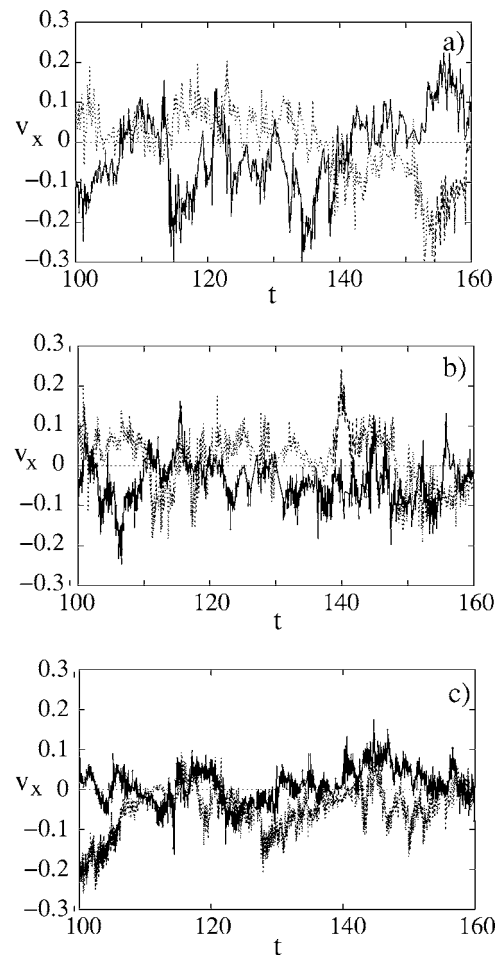
velocity fluctuations at the edge of boundary layers (estimated as the position of the peak in the root-mean-square velocity profile) remains constant when a mean flow structure is present, and decreases with Ra in the absence of a mean flow. The intensity of these fluctuations has to be compared with the mean horizontal wind, which is of the order of 10% of the free-fall velocity in the presence of large recirculations and even smaller in the flow regime of Fig. 2(b). This comparison suggests that fluctuations in the boundary layer are of the same order as the large-scale velocity, which itself is highly unsteady owing to frequent reversals, transitions from one state to another, and to azimuthal tilting of large structures. Even so, the time-averaged friction coefficients of Fig. 6(b), normalized by the maximum velocity (see inset of Fig. 1), are similar for the present boundary layers and for the flat plate. In addition, it is interesting that the friction coefficient, C_f, decreases with the boundary layer Reynolds number Re as Re$^{-1/2}$, as expected for laminar flows, and departs from it at higher Re, presumably marking the transition to turbulence. As an aside, for Pr=0.7, the transition value Ra$\approx 10^{12}$ agrees with the expression Ra$\approx 5.66 \times 10^{11}Pr^{1.4}/\Gamma^2 = 1.37 \times 10^{12}$ derived[12] for the maintenance of the fully developed turbulent state.
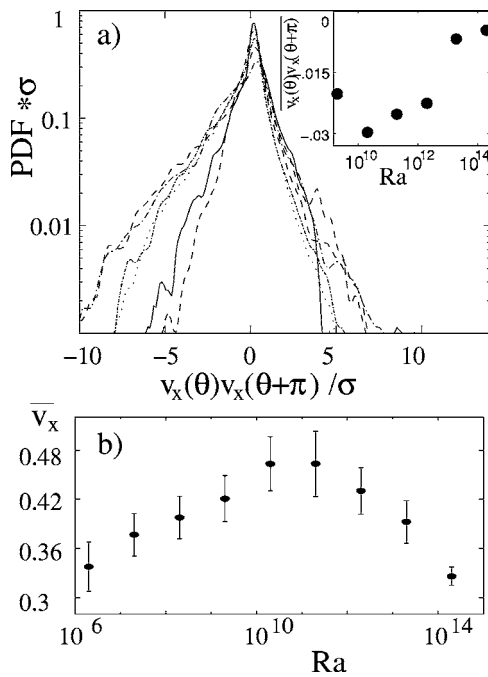
Although more results will have to await a forthcoming

FIG. 5. (a) Probability density function (PDF) of the product $v_x(\theta)v_x(\theta+\pi)$, the velocities being sampled in the positions of Fig. 3: (—) Ra=2×10¹⁴, (----) Ra=2×10¹³, (·······) Ra=2×10¹², (–·–) Ra=2×10¹¹, (----) Ra=2×10¹⁰, and (–·–) Ra=2×10⁹. The PDFs are normalized by the rms σ of $v_x(\theta)v_x(\theta+\pi)$. The inset shows the mean value of the correlation as functions of Ra. (b) Time average of the maximum vertical velocity as a function of the Rayleigh number for Pr=0.7.
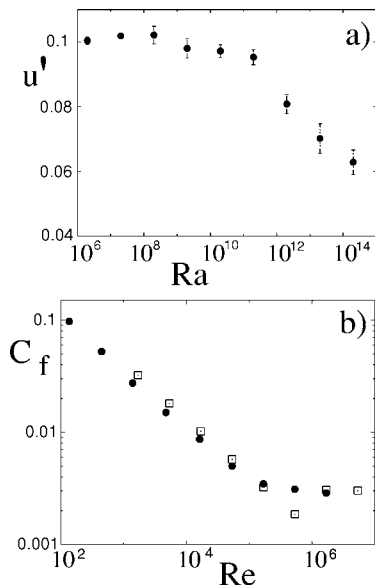

FIG. 6. (a) Velocity fluctuation at the edge of the kinematic boundary layers of the horizontal plates. (b) Friction coefficient at the horizontal plates: (●) present results, (□) data for the flat plate from Schlichting (Ref. 23). The Reynolds number Re is computed using the mean velocity at the edge of the viscous boundary layer. The friction coefficient is defined as the mean wall shear stress (averages are performed over the horizontal plates and in time) normalized by the factor Re/2.

paper, we can already conclude that for the present conditions the Nusselt number increases with the Rayleigh number following the 1/3 power law to some reasonable accuracy, at least in the range $2\times10^{10}\leqslant\mathrm{Ra}\leqslant2\times10^{14}$.

[1] D. Threlfall, "Free convection in low-temperature gaseous helium," J. Fluid Mech. **67**, 17 (1975).

[2] R. J. Goldstein and S. Tokuda, "Heat transfer by thermal convection at high Rayleigh numbers," Int. J. Heat Mass Transfer **23**, 738 (1979).

[3] X.-Z. Wu and A. Libchaber, "Scaling relations in thermal turbulence: The aspect-ratio dependence," Phys. Rev. A **45**, 842 (1992).

[4] B. Castaing, G. Gunaratne, F. Heslot, L. Kadanoff, A. Libchaber, S. Thomae, X.-Z. Wu, S. Zaleski, and G. Zanetti, "Scaling of hard thermal turbulence in Rayleigh-Bénard convection," J. Fluid Mech. **204**, 1 (1989).

[5] J. J. Niemela, L. Skrbek, K. R. Sreenivasan, and R. J. Donnely, "Turbulent convection at very high Rayleigh numbers," Nature (London) **404**, 837 (2000).

[6] X. Chavanne, F. Chillà, B. Chabaud, B. Castaing, and B. Hebral, "Turbulent Rayleigh-Bénard convection in gaseous and liquid He," Phys. Fluids **13**, 1300 (2001).

[7] P. E. Roche, B. Castaing, B. Chabaud, and B. Hebral, "Prandtl and Rayleigh numbers dependences in Rayleigh-Bènard convection," Europhys. Lett. **58**, 693 (2002).

[8] K. R. Sreenivasan and R. J. Donnelly, "Role of cryogenic helium in classical fluid dynamics: Basic research and model testing," Adv. Appl. Mech. **37**, 239 (2000).

[9] P. E. Roche, "Convection thermique turbulente en cellule de Rayleigh-Bènard cryogénique," Ph.D. thesis, Centre de Recherche sur les Trés Basses Températures Laboratoire CNRS associé á l'Université Joseph Fourier, 2000.

[10] G. Ahlers, "Effect of sidewall conductance on heat-transport measurements for turbulent Rayleigh-Benard convection," Phys. Rev. E **63**, 015303 (2001).

[11] R. Verzicco, "Side wall finite conductivity effects in confined turbulent thermal convection," J. Fluid Mech. **473**, 201 (2002).

[12] J. J. Niemela and K. R. Sreenivasan, "Confined turbulent convection," J. Fluid Mech. **481**, 355 (2003).

[13] R. Verzicco, "Effect of non-perfect thermal sources in turbulent thermal convection," Phys. Fluids **16**, 1965 (2004).

[14] E. Brown, A. Nikolaenko, D. Funfschilling, and G. Ahlers, "Heat transport in turbulent Rayleigh-Benard convection: Effect of finite top- and bottom-plate conductivity," Phys. Fluids **17**, 075108 (2005).

[15] S. Sun, K.-Q. Xia, and P. Tong, "Three-dimensional flow structures and dynamics of turbulent thermal convection in a cylindrical cell," Phys. Rev. E **72**, 026302 (2005).

[16] S. Grossmann and D. Lohse, "Scaling in thermal convection: a unifying theory," J. Fluid Mech. **407**, 27 (2000); "Thermal convection for large Prandtl number," Phys. Rev. Lett. **66**, 016305 (2002).

[17] R. Verzicco and R. Camussi, "Numerical experiments on strongly turbulent thermal convection in a slender cylindrical cell," J. Fluid Mech. **477**, 19 (2003).

[18] G. Grötzbach, "Spatial resolution requirements for direct numerical simulation of the Rayleigh-Bénard convection," J. Comput. Phys. **49**, 241 (1983).

[19] M. V. R. Malkus, "Heat transport and spectrum of thermal turbulence," Proc. R. Soc. London, Ser. A **225**, 196 (1954); C. H. B. Priestley, *Turbulent Transfer in the Lower Atmosphere* (University of Chicago Press, Chicago, 1959).

[20] A. Nikolaenko, E. Brown, D. Funfschilling, and G. Ahlers, "Heat transport by turbulent Rayleigh-Benard convection in cylindrical cells with aspect ratio one and less," J. Fluid Mech. **523**, 251 (2005).

[21] G. Stringano and R. Verzicco, "Mean flow structure in thermal convection in a cylindrical cell of aspect-ratio one half," J. Fluid Mech. (to be published).

[22] B. I. Shraiman and E. D. Siggia, "Heat transport in high Rayleigh number convection," Phys. Rev. A **42**, 3650 (1990).

[23] H. Schlichting, *Boundary Layer Theory* (McGraw-Hill, New York, 2000).